Probabilistic Engineering Mechanics 24 (2009) 117–127

Contents lists available at ScienceDirect

Probabilistic Engineering Mechanics

journal homepage: www.elsevier.com/locate/probengmech

Statistics and probabilistic modeling of simulated intergranular cracks

S.R. Arwade [a,*], M. Popat [b,1]

[a] University of Massachusetts, Amherst, Department of Civil and Environmental Engineering, Amherst, MA 01003, United States
[b] Citigroup, New York, NY, United States

ARTICLE INFO

Article history:
Received 22 June 2007
Received in revised form
26 March 2008
Accepted 31 March 2008
Available online 10 April 2008

Keywords:
Probabilistic fracture
Polycrystals
Statistics
Microcrack
Intergranular fracture

ABSTRACT

Using Monte Carlo simulation, the statistical properties of intergranular crack trajectories in polycrystalline materials are estimated. The polycrystalline microstructures are two dimensional and are modeled by a Poisson–Voronoi tessellation for the grain geometry and a uniform orientation distribution function for the crystallographic orientation. A heuristic is introduced for determining the path of crack propagation when the crack tip arrives at a grain boundary triple junction. This heuristic applies a combination of two criteria for determining the direction of crack propagation, the maximum circumferential stress criterion, and a criterion in which the crack is assumed to propagate in the direction with the least material resistance. The resistance of grain boundaries is assumed to be related to the crystallographic misorientation at the grain boundary. The trajectories of microcracks can be treated as a random process, and simulation results indicate that the crack process exhibits linear variance growth, the rate of which is related to the importance attached to the circumferential stress and the material resistance in determining the direction of propagation. The rate of variance growth is shown to vary with the average grain diameter, so that microcracks in polycrystals with small grain size will exhibit less spatial uncertainty. The statistics and distributions of the increments of the crack process are also given. Through a small change made to the normalization applied to non-dimensionalize the statistics, the results are extended to polycrystals that have spatially varying grain size. Finally, a probabilistic model is proposed that is able to produce synthetic crack trajectories that replicate the important statistical properties of the simulated cracks. Such a model may prove useful in studies of the transition from micro to macrocracking.

1. Introduction

Uncertainty in fracture phenomena can be traced to two sources, uncertainty in loading and uncertainty in material properties. The latter of these is particularly significant when cracks are microstructurally small, that is, when the length of the crack is comparable to a length scale of the material microstructure. An example would be a crack in a polycrystalline material the length of which is only a few times the average grain diameter. Uncertainty in microcrack propagation can be particularly important since a large portion of the service lifetime of typical structural components is consumed by the initiation and short crack growth regimes. In this paper, Monte Carlo simulation is used to evaluate the uncertainty of intergranular microcrack trajectories in two-dimensional polycrystalline materials.

The problem of microcrack initiation and growth has received a large amount of attention in recent years from experimental, analytical, and computational researchers. Most relevant of the experimental investigations to this work is the finding that the statistics of cracks in concrete exhibit features of Brownian motion processes, and that the tortuosity of the crack path is related to the fracture toughness [1]. Regarding initiation of microcracks, successful models have been developed for the nucleation and growth of voids on grain boundaries [2,3], and cohesive finite elements have been used to model the separation of material at grain boundaries [4–6]. Significant advances have been made in the ability to simulate, with high fidelity, the mechanics of fracture initiation in polycrystalline materials [7]. The more general topic of spatial distribution and geometry of damage in random media is also now coming under study using approximate, but highly efficient methods [8,9].

Related directly to the problem of uncertainty in fracture problems are two sets of ongoing studies that seek to provide high fidelity simulation capabilities for probabilistic nonlinear crack growth in heterogeneous materials [10–12]. While the rate of progress in the modeling of highly nonlinear fracture phenomena in heterogeneous materials is impressive, the progress

* Corresponding address: University of Massachusetts, Department of Civil and Environmental Engineering, 223 Marston Hall, Amherst, MA 01003, United States. Tel.: +1 413 577 0926.
E-mail address: arwade@ecs.umass.edu (S.R. Arwade).
[1] Formerly graduate student, Department of Civil Engineering, Johns Hopkins University, United States.

0266-8920/$ – see front matter © 2008 Elsevier Ltd. All rights reserved.
doi:10.1016/j.probengmech.2008.03.002

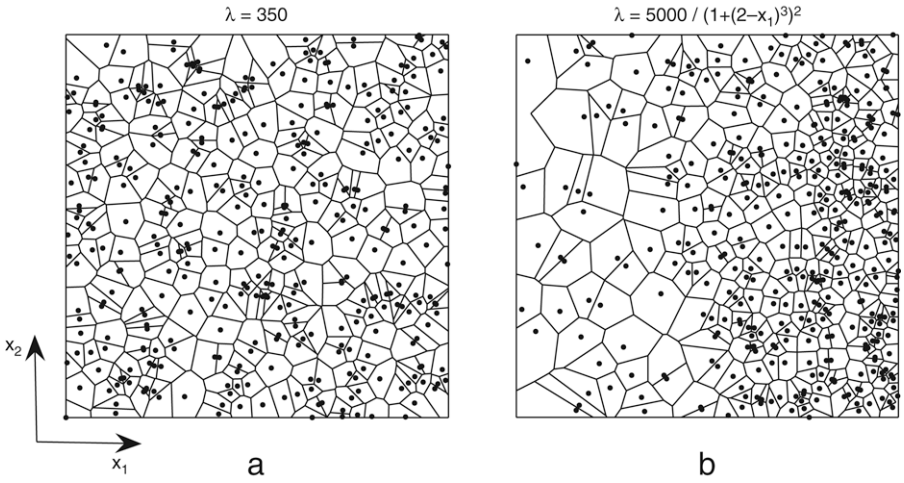

Fig. 1. Example of Voronoi tessellations with (a) homogeneous average grain size, and (b) inhomogeneous average grain size.

comes at the cost of increased demand on computational resources. One approach to ameliorating this increasing demand on computational resources has been to show that crack growth in random media is largely independent of the details of the crack trajectory, and that the stress intensity factors depend almost entirely on the geometry of the final kink in the crack path [13,14].

In this paper, simplifying assumptions are introduced regarding the mechanics of fracture that allow the very rapid evaluation of intergranular fracture paths in two-dimensional polycrystals. The paper begins with a description of the microstructural model, and then proceeds to introduce a heuristic for crack propagation that is based on simplified representations of the stress field in the microstructure and the grain boundary material resistance. Using this heuristic, a Monte Carlo study is performed, the results of which are used to give a thorough statistical description of the crack path process for intergranular fracture of polycrystals subject to uniaxial loading. Lastly, a probabilistic model is proposed that can be used to generate statistically realistic microcrack trajectories without the need to generate a sample microstructure or perform even an approximate fracture analysis.

2. Microstructure model

This paper addresses the growth of cracks in brittle polycrystalline materials in two dimensions. A common model for the microstructure of such materials is the Voronoi tessellation [15]. The two-dimensional Voronoi tessellation is used here as a model for the microstructure of a polycrystalline material comprising grains with statistically isotropic shape. The Voronoi tessellation partitions a domain D into n cells, or polygons, determined by an underlying set of points $\{\mathbf{c}_i\}$ called the nuclei. The polygons that make up the tessellation comprise the sets of points that are closer to one nucleus than any other. To put this more formally, the polygon P_i associated with nucleus $\mathbf{c}_i$ is the set of points

$$P_i = \{\mathbf{x} \in D : ||\mathbf{x} - \mathbf{c}_i|| < ||\mathbf{x} - \mathbf{c}_j||\} \quad \forall j \neq i. \tag{1}$$

The two-dimensional Voronoi tessellation is a consistent model for materials that obey the physical assumptions that (1) grain nucleation is simultaneous, (2) grain growth is isotropic and occurs at a constant rate, and (3) the grains resulting from the solidification process are (non-circular) cylinders. The third physical assumption is satisfied in thin films in which the thickness is small compared to the grain size, or in thick materials in which the conditions of solidification are such that columnar grains form. The Voronoi tessellation is also a valid model only for those polycrystalline materials that have not undergone significant inelastic deformation following solidification. Large inelastic deformations distort the grains so that they are not equiaxed and do not have isotropic shape.

The Voronoi tessellation gives a unique partitioning of D for a given set of nuclei $\{\mathbf{c}_i\}$ so that control over the tessellation resides in the model used for placement of the nuclei. If deterministic nucleus locations are used, for example nuclei lying on a cubic grid, then the tessellation itself is rendered deterministic. Here, in order to model random material microstructures, the Poisson point field $N(D)$ is used as a model for the nucleation sites. The two-dimensional Poisson point field is governed by its intensity function $\lambda(\mathbf{x}), \mathbf{x} \in \mathbb{R}^2$ which has dimension L^{-2} and gives the expected number of points per unit area at location $\mathbf{x}$. It can alternatively be loosely interpreted as the likelihood that a point will be found at location $\mathbf{x}$. The expected number of points in D is given by $E[N(D)] = \bar{N} = \int_D \lambda(\mathbf{x})\mathrm{d}\mathbf{x}$, and the random variable $N(D)$ is Poisson distributed with parameter $\bar{N}$. For the case of a homogeneous Poisson point field, where $\lambda(\mathbf{x}) = \lambda$, $\bar{N} = \lambda A$, where $A = \int_D \mathrm{d}\mathbf{x}$ is the area of D. Numerous algorithms are available for generating realizations of homogeneous and inhomogeneous Poisson point field [15]; the thinning algorithm is implemented here. Fig. 1 shows examples of the two grain geometry models used in this study, one with spatially homogeneous grain size $\lambda = 350$ and one with grain size decreasing with x_1 as $\lambda = 5000/(1 + (2 - x_1)^3)^2$. In both cases, $D = [0, 1]^2$ is the unit square and $\bar{N} = 350$.

The crystallographic orientation forms the second part of the microstructural model used in this work. While only two-dimensional grain geometries are considered here, the full, three-dimensional representation of the orientation is used. The crystallographic orientation gives the rotation necessary to bring the crystal axes into coincidence with a reference coordinate system. The crystal axes are typically defined with respect to the atomic positions on the periodic crystal lattice of the material, and define the principal axes of material anisotropy. The misorientation is the difference in orientation between two sets of crystal axes and is critical in defining the nature of grain boundaries. Of the many possible representations of the crystallographic orientation [16], the Euler angles (ϕ_1, Φ, ϕ_2) [17] are used here to define the orientation with the notation $\Psi_1 = \phi_1, \Psi_2 = \Phi, \Psi_3 = \phi_2$ adopted to allow the orientation to be denoted by the vector $\mathbf{\Psi}$. Capitalization of $\{\Psi_i\}$ and $\mathbf{\Psi}$ indicates that these are random quantities. The misorientation, on the other hand, is represented here in its axis/angle form, in which $\Theta(\mathbf{\Psi}_i, \mathbf{\Psi}_j) = \Theta_{ij}$ is the angle of misorientation between the orientation in grains i and j. Capitalization is again used to indicate

that the misorientation is a random quantity by virtue of the uncertainty associated with the orientation field.

The orientation is assumed to be constant within grains so that the orientation field $\boldsymbol{\Psi}(\mathbf{x})$ throughout a virtual polycrystal with n grains is determined by the random vectors $\boldsymbol{\Psi}_k = \boldsymbol{\Psi}(\mathbf{c}_k), k = 1, \ldots, n$ which are here assumed to be uncorrelated. Since the effect of crystallographic texture is not a subject of study in this work, the marginal distributions of $\boldsymbol{\Psi}(\mathbf{x})$ are defined such that

$$\begin{aligned} &\Psi_1 \sim U(0, 2\pi) \\ &\frac{1-\cos(\Psi_2)}{2} \sim U(0, 1) \\ &\Psi_3 \sim U(0, 2\pi) \end{aligned} \tag{2}$$

which give orientations that are uniformly distributed on the stereographic sphere. Uncorrelated orientations with marginal distributions given by Eq. (2) result in grain boundary misorientations Θ_{ij} that follow the Mackenzie distribution [16]. This distribution is itself non-uniform, with maximal probability density near 45°. Non-uniformity of the misorientation distribution function has implications for the mechanics of intergranular fracture since the strength of grain boundaries can be linked to the misorientation.

3. Crack propagation heuristic

The above model for a two-dimensional polycrystalline microstructure with uniformly distributed crystallographic orientations is developed for use in investigating the propagation of intergranular cracks. Since crack trajectories $C(x_1)$ through such microstructures, and subject to the boundary conditions corresponding to a macroscopic uniaxial strain field, will be random, and since the main goal of this paper is to describe the statistical properties of such cracks, Monte Carlo simulation is used to generate a large number of virtual cracks from which statistics can be estimated. One set of assumptions regarding fracture behavior in the problem is:

(1) material failure is brittle and linear elastic fracture mechanics applies,
(2) the crack is intergranular, that is, $C(x_1)$ always lies on a grain boundary,
(3) cracks initiate at the left edge of D, or $x_1 = 0$,
(4) crack propagation is always in the direction of increasing x_1,
(5) cracks do not branch,
(6) crack propagation continues until the crack tip reaches $x_1 = 1$, or the right edge of D.

Subject to the preceding assumptions, determination of the fracture path through D requires the determination of the site of crack initiation from among the points of intersection of the grain boundary network with $x_1 = 0$, and, subsequent to that determination, the identification, at a series of grain boundary junctions (triple points), of the grain boundary along which the crack propagates. If the grain boundary vertices are denoted by $\{\mathbf{v}_i\}$, and those that satisfy $v_{i,1} = 0$ are denoted by $\mathbf{v}_j^0$ the initiation site is chosen as

$$C(0) = \mathbf{v}_{j,2}, \quad j = \arg\min_j \left(\|\mathbf{v}_j^0 - [0, 0.5]^{\mathrm{T}}\| \right) \tag{3}$$

so that the crack begins as close as possible to the middle of the left edge of D. This assumption regarding the initiation site does not affect the post-initiation behavior of the cracks, and is made without sacrificing generality of the results.

The key simplifying assumption made here is that crack growth is strictly intergranular, meaning that the crack surface always coincides with grain boundaries. Crack growth in brittle materials proceeds along the grain boundaries when the strength, or toughness, of the boundary is substantially lower than that of the crystalline material that makes up the individual grains. If, conversely, the boundary phase has greater toughness than the crystalline phase, cracks will tend to propagate through the grains. This mode of crack growth is called transgranular fracture.

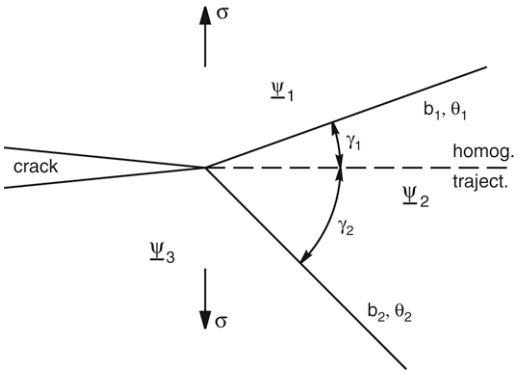

Fig. 2. Typical microstructural geometry at the time when a crack tip approaches a grain boundary triple point.

Generally, it is the presence of defects or localized weakening that drives crack growth to the grain boundaries. For example, a material with a large number of second phase particles located at grain boundary surfaces may exhibit intergranular fracture due to stress concentration at the grain boundaries induced by the presence of the second phase particles. Similarly, if voids have nucleated and grown on the grain boundaries, as, for example, during some high-temperature deformation processes, these voids provide a low-energy pathway for crack propagation along the grain boundaries. Finally, during plastic deformation dislocations can accumulate at grain boundaries. These accumulations of dislocations act as defects and can induce intergranular fracture. Grain boundaries can also be weakened by chemical processes that preferentially attack the boundary phase. Fracture under these conditions is called stress corrosion cracking. Similar grain boundary weakening occurs during hydrogen embrittlement of metals. Generally speaking, second phase particles and voids can lead to intergranular fracture in metals and ceramics, whereas dislocation pileup, stress corrosion and hydrogen embrittlement drive intergranular fracture in metals. Two specific examples are the occurrence of stress corrosion cracking in aluminum alloys employed in airframe structures, and hydrogen embrittlement fracture in high-strength steels used in the nuclear industry.

The above discussion shows that the intergranular fracture mode studied in this paper is important in a broad range of engineering situations. The transgranular mode, clearly, is also an important fracture mode in engineered structures. The simplified approaches to trajectory determination described here can in principle be extended to simulate transgranular fracture. This extension, however, would require a reliable method for calculating the relative toughness of grain boundary and crystalline phases. This is much more challenging than what is required here, namely the relative toughness of two grain boundaries. Furthermore, the assumption of intergranular fracture presents a discrete set of possible trajectories, following the grain boundaries. Transgranular crack trajectories can vary continuously, resulting in an infinite set of possible trajectories. Practically speaking, these complications would significantly reduce the efficiency and utility a model for transgranular fracture analogous to that proposed here for intergranular fracture.

Fig. 2 shows the typical situation that arises when the crack tip has completed propagation along a grain boundary and has arrived at a triple point of the grain boundary network. In the figure, the three grains forming the triple point are given the indices 1, 2, 3. The boundaries are denoted by $b_i, i = 1, 2$, with the misorientation angle at the boundary being $\theta_i, i = 1, 2$. These misorientations

are calculated from the grain crystallographic orientations $\Psi_j, j = 1, 2, 3$. The macroscopic stress field is shown as the tensile stress σ, and the homogeneous trajectory is the direction the crack would propagate in a homogeneous, isotropic, continuum subject to this applied macroscopic stress state. The angles γ_1 and γ_2 give the deviation from the homogeneous trajectory of the candidate crack paths defined by the grain boundaries.

In linear elastic fracture mechanics cracks are assumed to propagate in the direction of maximum circumferential stress, the σ_θ-max assumption, or, alternatively, the direction of maximum energy release rate, the G-max assumption, among several other possibilities [18]. In the current situation of an intergranular crack tip at a triple point, at most two candidate directions are available, coinciding with the boundaries b_1 and b_2. Using finite element analysis, the circumferential stress could be calculated, which, at b_1 and b_2 is equivalent to the stress component normal to the boundary, denoted here by σ_{n1} and σ_{n2} for the two boundaries. Alternatively, using an additional finite element analysis for each candidate direction, a finite difference approximation of the energy release rate in each of the candidate directions can be obtained.

This approach has been previously implemented for the type of problem addressed in this paper [19]. This approach requires, however, three finite element analyses at each decision point of the crack propagation, as well as significant challenging remeshing. Thus, this finite element based approach to crack trajectory determination is not practical for the Monte Carlo simulation of crack geometry proposed in this study.

In order to obtain meaningful results regarding the geometry of intergranular cracks via Monte Carlo simulation, an heuristic model for determining the direction of crack propagation at triple junctions is now proposed (see also [20]) that allows for rapid computation of fracture patterns in random polycrystalline materials. Define, for each grain boundary, or candidate direction, the quantity

$$A_i = w\left(1 - \frac{|\cos\gamma_i|}{1}\right) + (1-w)\left(1 - \frac{\theta_i}{\theta_{\max}}\right) \tag{4}$$

where γ_i and θ_i are defined as in Fig. 2, 1 is the maximum value of $\cos\gamma_i$, $\theta_{\max} = 62.8^\circ$ is the maximum angle of misorientation permissible in the axis/angle representation, and w is a weight factor between the two competing criteria. The direction of crack propagation from a triple point is chosen to minimize A. When $w = 1$, $A_i = 1 - \cos\gamma_i$ which is minimized for $\gamma_i = 0$. Thus, when $w = 1$, the criterion reduces to one approximating the σ_θ-max criterion with $\sigma_{n1} = \sigma\cos\gamma_1$ and $\sigma_{n2} = \sigma\cos\gamma_2$. These expressions approximate the actual circumferential stresses that arise at the crack tip using the assumption that the state of stress at the triple point is $\sigma_{22} = \sigma$, $\sigma_{11} = \sigma_{12} = 0$. These assumptions correspond to neglecting the stress field heterogeneities induced by the elastic mismatch between the individual grains resulting from the variation of orientation. This reduces the problem of calculation of the stresses σ_{n1} and σ_{n2} to the calculation of traction on a surface of known orientation in a known stress field, as opposed to a finite element analysis of a heterogeneous medium. For materials such as aluminum, with a relatively small degree of anisotropy, this assumption is close to being valid. For materials with more severe anisotropy the assumption may not be appropriate.

Conversely, when $w = 0$, the stresses σ_{n1} and σ_{n2} are neglected completely, and only the grain boundary misorientation is considered in determining the direction of crack propagation. This criterion is based on the observation that the fracture toughness of grain boundaries is inversely related to the angle of misorientation. That is, grain boundaries with large misorientation tend to be less resistant to fracture than those with small misorientation [21,22]. The relationship between orientation and fracture toughness is complicated, and has not been fully explored either by experiments or direct calculations. For example, there exists a class of special grain boundaries that exhibit extremely high strength despite relatively large angles of misorientation. The details of this relationship depend on the complicated geometry of the intersection of the crystal lattices. For the purposes of this study, the details of the misorientation–toughness relationship are neglected, and it is assumed that the relationship is linear.

To summarize, when $w = 1$ the crack direction is determined based on maximization of the approximate normalized resolved normal stress on the boundary, given by $\cos\gamma_i$ if the remote stress is of unit magnitude, and when $w = 0$, the crack direction is determined based on maximization of the grain boundary misorientation, corresponding to a minimization of the grain boundary fracture toughness. The two criteria at the extremes of the range of w are based on selecting either the most heavily loaded grain boundary ($w = 1$), or the weakest grain boundary ($w = 0$). The maximum normal stress criterion delivers crack paths that remain as close as possible to the homogeneous trajectory, while, for uncorrelated orientations, the maximum misorientation criterion results in equal probability of crack advance along each of the two candidate grain boundaries when a crack encounters a triple point, subject to the constraint that the crack tip move in the direction of increasing x_1.

4. Results and discussion

The crack propagation heuristic described above is implemented in `MATLAB` to solve the crack trajectory in a simulated polycrystal. This section presents the results of Monte Carlo simulation of these crack trajectories. The geometry of the polycrystal is $D = [0, 1]^2$ mm, and a macroscopic stress field is assumed that has $\sigma_{22} = \sigma$, $\sigma_{11} = 0$, and $\sigma_{12} = 0$. As described in the previous section, the crack is assumed to initiate at $x_1 = 0$ with $C(0)$ as close as possible to $x_2 = 0.5$. Since this paper is focused on the uncertainty associated with microcrack propagation, rather than microcrack initiation, all simulated crack trajectories are shifted in the x_2 direction so that they initiate from $(0, 0.5)$ exactly. If the simulated crack trajectory is $C(x_1)$, then the shifted crack trajectory is $C(x_1) - (C(0) - 0.5)$. Only the shifted crack trajectories are discussed in this paper, so, to simplify the notation, $C(x_1)$ is used to denote the shifted crack paths.

Results are given in this section for two types of polycrystals, one with a spatially homogeneous average grain size corresponding to $\lambda(\mathbf{x}) = \lambda$, and one with a spatially varying average grain size corresponding to $\lambda(\mathbf{x}) = 5000/(1 + (2 - x_2)^3)^2$. This last intensity function is arbitrarily chosen, but gives grain structures that are representative of those that arise in materials subject to differential cooling and solidification.

4.1. Trajectory variance

Statistics of the random process $C(x_1)$ can be estimated from the realizations generated by the Monte Carlo algorithm described above. This section, dealing with simulated polycrystals with constant grain intensity, examines the variability of these statistics with the grain intensity λ and the propagation criterion parameter w.

Fig. 3 shows 25 crack trajectory realizations for $\lambda = 1000$ and (a) $w = 0$ and (b) $w = 1$, corresponding to the maximum misorientation and maximum normal stress criteria respectively. As expected, the cracks generated from the maximum normal stress criterion, always preferring to remain close to the homogeneous trajectory, exhibit significantly less scatter than those generated using the maximum misorientation criterion.

The first observation corresponding to the statistical character of these crack trajectories is that $\mathrm{var}[C(x_1)] = \sigma^2(x_1)$, the variance

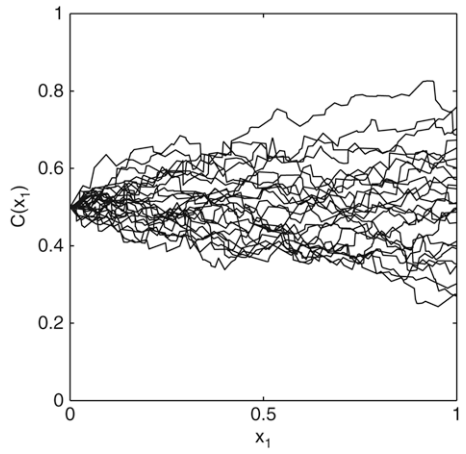

(a) $w = 0$; max. misorientation.

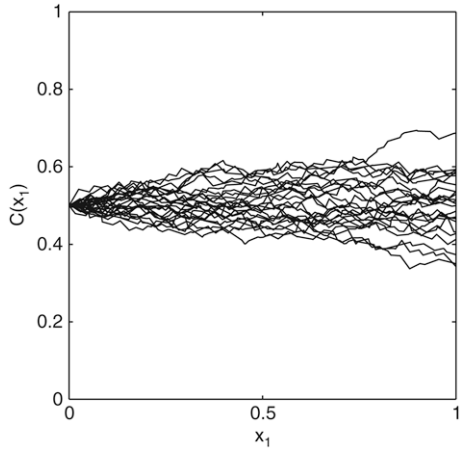

(b) $w = 1$; max. normal stress.

Fig. 3. Sample Monte Carlo crack paths for (a) maximum misorientation criterion, and (b) maximum normal stress criterion.

of the crack process, grows linearly with x_1. This is shown in Fig. 4, which shows $\sigma^2(x_1)$ for polycrystals with $\lambda = 1000$ and values of w ranging from 0 to 1. As previously observed, the variance grows faster for small w. The slope of the lines in Fig. 4 are the statistical signature of intergranular growth according to Eq. (4), and the determination of how this slope depends on the parameters λ and w forms the core of this section. Each of the lines plotted is determined from 5000 independent crack path realizations, so that the figure contains data from 55 000 simulated crack paths.

The axes in Fig. 4 are horizontal position x_1 in millimeters, and the variance of the crack trajectory, having units of mm^2. If the results of this study are to be broadly applicable, they should, where possible, be presented in non-dimensional form. The normalizing length scale in the problem is $\lambda^{-1/2}$, which is related to the average grain size $\bar{A}$ since $\bar{A} \propto \lambda^{-1}$. To non-dimensionalize the results, let $s^2 = \sigma^2\lambda$ and $\tilde{x_1} = \int_0^{x_1} \sqrt{\lambda}\,\mathrm{d}u = x_1\sqrt{\lambda}$. To see the relationship between the slope of the normalized variance, $\dot{s}^2 = \mathrm{d}s^2/\mathrm{d}\tilde{x_1}$, and the rate of increase, $\mathrm{d}\sigma^2/\mathrm{d}x_1$, of the raw variance, observe that

$$\frac{\mathrm{d}s^2}{\mathrm{d}\tilde{x}_1} = \frac{\mathrm{d}s^2}{\mathrm{d}x_1}\frac{\mathrm{d}x_1}{\mathrm{d}\tilde{x}_1} = \frac{\mathrm{d}\sigma^2}{\mathrm{d}x_1}\sqrt{\lambda}. \tag{5}$$

Intuition suggests that the quantity $\dot{s}^2$ should be a constant $C_s(w)$ for fixed w, in which case

$$C_s(w) = \frac{\mathrm{d}\sigma^2}{\mathrm{d}x_1}\sqrt{\lambda}. \tag{6}$$

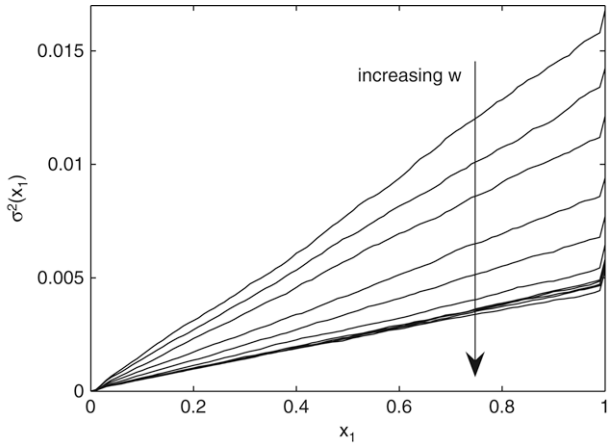

Fig. 4. Crack variance for $\lambda = 1000$ and $w = [0, 0.1, \ldots, 1]$. The figure shows the linearity of the variance growth as well as the dependence on the rate of variance growth on the parameter w.

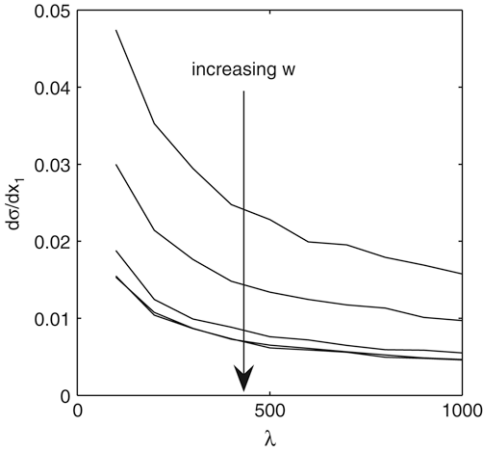

(a) raw variance growth.

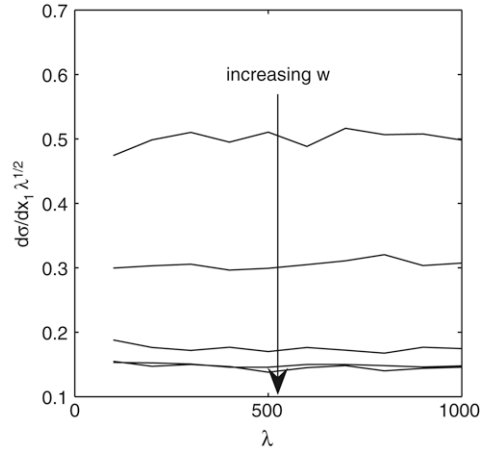

(b) normalized variance growth

Fig. 5. Crack process (a) raw and (b) normalized, variance growth for values $w = [0, 0.25, 0.5, 0.75, 1]$, and intensity values $\lambda = [100, 200, \ldots, 1000]$.

This is shown in Fig. 5 in which the normalization is applied to the slope of the variance growth to remove the dependence on the intensity. The data presented in Fig. 5 are obtained from the Monte Carlo simulation described above. In the data, there is a boundary effect in which the variance growth becomes nonlinear near $x_1 = 0$ and $x_1 = 1$ (see Fig. 4). In determining the slopes of the variance

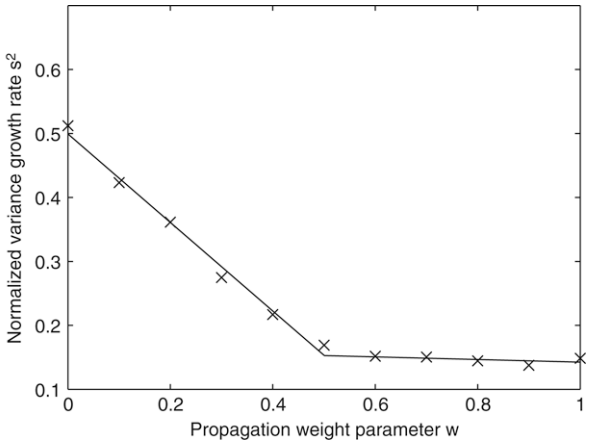

Fig. 6. Normalized crack variance growth rate against propagation weight parameter for $\lambda = 1000$.

curves, this boundary effect is ignored, and least squares regression gives the best linear fit $\sigma^2 = \dot{\sigma}^2 x_1$ to the data in the interval $[\bar{d}_\epsilon, 1-\bar{d}_\epsilon]$ where $\bar{d}_\epsilon = 2\sqrt{1/\lambda\pi}$ is the average grain diameter. This figure, along with the above calculations, demonstrates that the rate of variance growth, a quantification of the uncertainty in crack trajectory, increases with decreasing grain intensity, and, when normalized by multiplication by the square root of the intensity, is constant. This normalization does not remove the dependence on the parameter w. The alternative interpretation of these statements is that the crack path variance growth rate must be normalized by division by the square root of the average grain size, and that crack trajectories are less scattered in materials with small grain sizes.

Returning to the data of Fig. 4, 6 shows the variation of the normalized rate of variance growth $\dot{s}^2 = \dot{\sigma}^2\sqrt{\lambda}$ with the propagation weight criterion w. The variance growth rate drops precipitously with increasing w, nearly reaching its limiting value of approximately 0.15 near $x_1 = 0.5$. The weight parameter w can be interpreted as a property of the polycrystalline material, although a formal connection between w and the material properties such as the misorientation distribution function and the grain boundary fracture toughness remains to be derived.

The data in Fig. 6 are shown overlaid with a bilinear fit that yields the approximate functional relationship

$$\dot{s}^2 = \begin{cases} -0.69w + 0.50, & 0 < w \le 0.5 \\ -0.020w + 0.16, & 0.5 < w \le 1. \end{cases} \tag{7}$$

Having the relation between $\dot{s}^2$ and w in an, at least approximate, functional form, will prove useful when a method is later proposed for directly simulating intergranular crack trajectories.

4.2. Trajectory increments

While the results presented above give a characterization of the variability of the entire crack path, also important are finer scale details of the crack path statistics, namely the marginal distributions of the crack path process, the distributions of the increments of the crack process, and the correlation structure of the crack process. The crack process $C(x_1)$ is piecewise linear because the cracks are intergranular and the Voronoi tessellation produces polygonal grains. Therefore, the process of crack advance can be viewed as an incremental process

$$\begin{aligned} x_{1,i+1} &= x_{1,i} + \Delta X_1, \\ C(x_{1,i+1}) &= C(x_{1,i}) + \Delta X_2 \end{aligned} \tag{8}$$

in which ΔX_1 and ΔX_2 are random variables. The properties of the random variables ΔX_1 and ΔX_2 should depend upon the system parameters w and λ. Fig. 7 shows typical histograms for the crack process increments for $w = 0.5$ and $\lambda = 500$. Weibull and exponential fits to the Δx_1 data are given. For the Δx_2 data, the density $f(x) = \nu \exp(-\nu|x|)/2$ with $\nu^{-1} = E[|\Delta x_2|]$ provides a good fit and is called herein the two-sided exponential distribution. The fit of the Weibull and exponential distributions to the Δx_1 data is not very good, particularly in the positive tail of the distribution, where both the Weibull and exponential overpredict the number of large values of Δx_1. The exponential distribution, however, has the disadvantage of drastically overpredicting the number of very small increments of crack advance. Therefore, the Weibull pdf is selected as the model for the random variable ΔX_1. It is important to note that the Weibull distribution is chosen merely because it provides the best fit to the data of the standard library of probability distributions, and not because of any connection of ΔX_1 to the assumptions of extreme value behavior that underlie the Weibull distribution. Alternatively, one could use the empirical cdf estimated from the MC simulation results. For the Δx_2 data, the two-sided exponential distribution with parameter ν, mean zero and variance $2/\nu^2$, provides a good qualitative fit, though, as with the Δx_1 data, the tails are heavier than the data indicate.

The histograms shown in Fig. 7 are typical in shape for the random variables Δx_1 and Δx_2 across the range of values $w = [0, 1]$ and $\lambda = [100, 1000]$ investigated here. The mean and standard deviation of the crack increments, when normalized by multiplication by the square root of the intensity, are found to be constant across variation in intensity λ. The mean and standard deviation of the crack increments do, however, vary with the propagation parameter w. This is shown in Fig. 8(a) which shows the mean and standard deviation of ΔX_1 increasing with increasing w, as crack trajectories are forced closer to the homogeneous

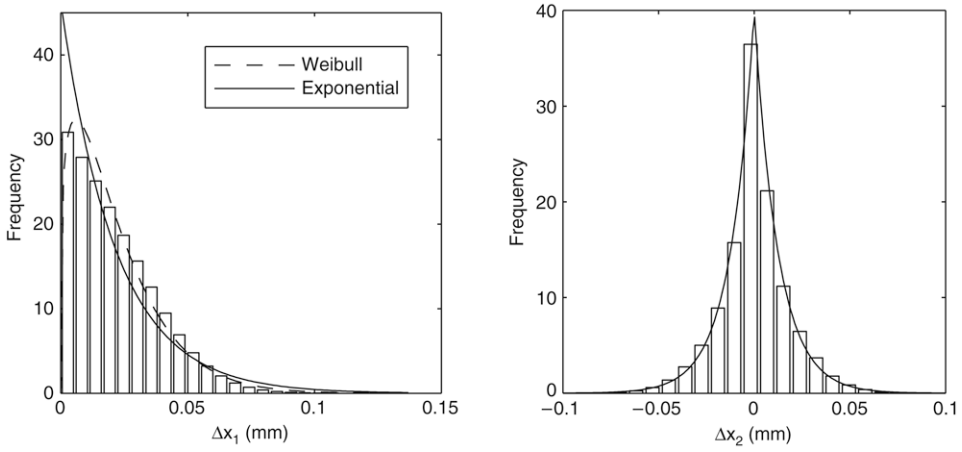

Fig. 7. Histograms and estimated probability density functions for the crack advance increments with $w = 0.5$ and $\lambda = 500$.

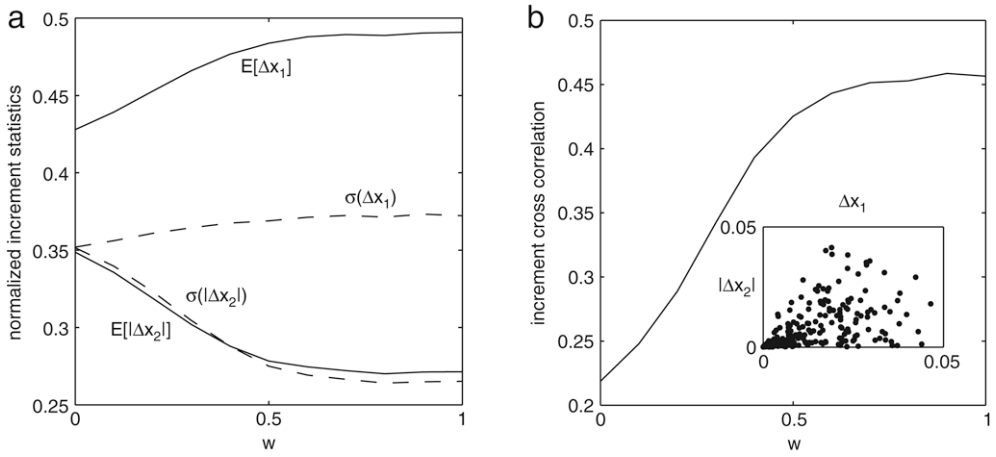

Fig. 8. Crack increment statistics: (a) mean and standard deviation of ΔX_1 and $|\Delta X_2|$; (b) crack increment cross correlation and scatter plot.

trajectory, and conversely, the mean and standard deviation of $|\Delta X_2|$ decreasing with increasing w.

The variables ΔX_1 and ΔX_2 are uncorrelated, with a maximum estimated correlation coefficient of 0.002 based on 500 000 variable pairs. The variables ΔX_1 and $|\Delta X_2|$, however, are not uncorrelated. Fig. 8(b) shows the dependence of the correlation coefficient on the propagation parameter w, along with a scatter plot of ΔX_1 and $|\Delta X_2|$ for $w = 1$ and $\lambda = 1000$. As w increases, the maximum normal stress criterion becoming increasingly significant in determining the trajectory, the correlation of the crack increments increases to a maximum value of approximately 0.46. This correlation is significant and is critical in generating realistic realizations of the crack process $C(x_1)$.

The spatial correlation structure of the crack process can be given in two ways. In one, correlation between the crack process increments is used to characterize the process, and in the other, $C(x_1)$ is treated as a continuous process with a correlation function that depends on two position variables. In the first approach the correlation structure is given by the matrix scaled covariance function with components

$$\rho_{ij}(n) = \frac{(E[\Delta x_{i,k}] - \mu_{\Delta x_i})(E[\Delta x_{j,k+n}] - \mu_{\Delta x_j})}{\sigma_{\Delta x_i}\sigma_{\Delta x_j}}. \tag{9}$$

The Monte Carlo data show that, for $n \geq 2$, $\rho_{ij}(n) \approx 0$, and that $\rho_{12}(1) \approx 0$. Fig. 8(b) gives $\rho_{1|2|}(1)$, where the bars around the 2 indicate that the absolute value of ΔX_2 has been used in the calculation, and Fig. 9 gives $\rho_{ii}(1), i = 1, 2$, in addition to $\rho_{12}(n)$, which is near zero. The correlations in Fig. 9 are everywhere negative, indicating that short increments of crack advance are likely to be followed by long increments, and vice versa. The magnitude of the correlations shown in Figs. 8(b) and 9 grows with w, indicating that as the crack paths are forced to remain closer to the homogeneous trajectory, the correlation increases.

The second way to characterize the correlation structure is through a continuous scaled covariance function

$$\mathrm{cov}(y, z) = E[C(y) - \mu_c]E[C(z) - \mu_c]. \tag{10}$$

If $y < z$, this expression can be rewritten as

$$\begin{aligned}\mathrm{cov}(y, z) &= E[(C(z) - C(y) + C(y))\,C(y)] - \mu_c^2 \\ &= E[(C(z) - C(y))\,C(y)] + E[C(y)^2] - \mu_c^2 \\ &\approx \dot{\sigma}^2(\lambda, w)y \end{aligned} \tag{11}$$

where the third step results only in an approximate equality because the increment $C(z) - C(y)$ is not strictly independent of $C(y)$ for the crack process. In Eq. (11), $\dot{\sigma}^2(\lambda, w) = \dot{s}^2(w)/\sqrt{\lambda}$ is the rate of variance growth of the crack process, and $\dot{s}^2(w)$ can be found from Eq. (7) or Fig. 6. If $z < y$ the calculations of Eq. (11) can be repeated, resulting in $\mathrm{cov}(y, z) \approx \dot{\sigma}^2(\lambda, w)z$, so that the final covariance function is

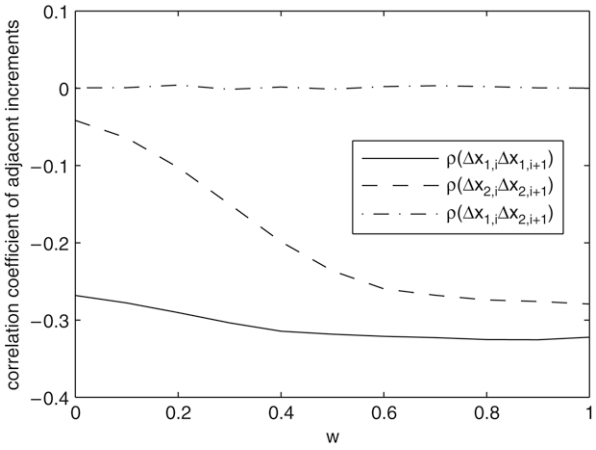

Fig. 9. Crack increment scaled covariance for sequential increments.

$$\mathrm{cov}(y, z) \approx \frac{\dot{s}^2(w)}{\sqrt{\lambda}} \min(y, z), \tag{12}$$

which is, excepting a scale factor, equal to the covariance function of the Brownian motion process $\mathrm{cov}_B(y, z) = \min(y, z)$. Fig. 10 shows, (a) the covariance function of the crack process for $w = 0.5$ and $\lambda = 1000$ based on 5000 Monte Carlo simulations, and (b) the difference between the estimated covariance of Fig. 10(a) and the approximate analytical function of Eq. (11). The agreement is excellent, with a maximum deviation of 1×10^{-3}. This deviation is, however, highly localized near $y = z = 1$, where it has been previously shown that a boundary effect introduces error into the Monte Carlo results. Elsewhere, the error is of the order of 1×10^{-4}.

4.3. Trajectory marginal distributions

The crack process $C(x_1)$ can be viewed as a sum of random variables $C(x_1) = \sum_{k=1}^{m} \Delta X_{2,k}$ where m is determined by how many grain boundary triple junctions have been traversed by the crack tip. If the random variables $\{\Delta X_{2,k}\}$ were identically distributed and independent, the central limit theorem would indicate that the marginal distribution of $C(x_1)$ should approach the Gaussian distribution for sufficiently large values of x_1. In this problem, these variables are not independent (see Fig. 9). Nevertheless, Fig. 11 indicates that convergence to a Gaussian marginal distribution

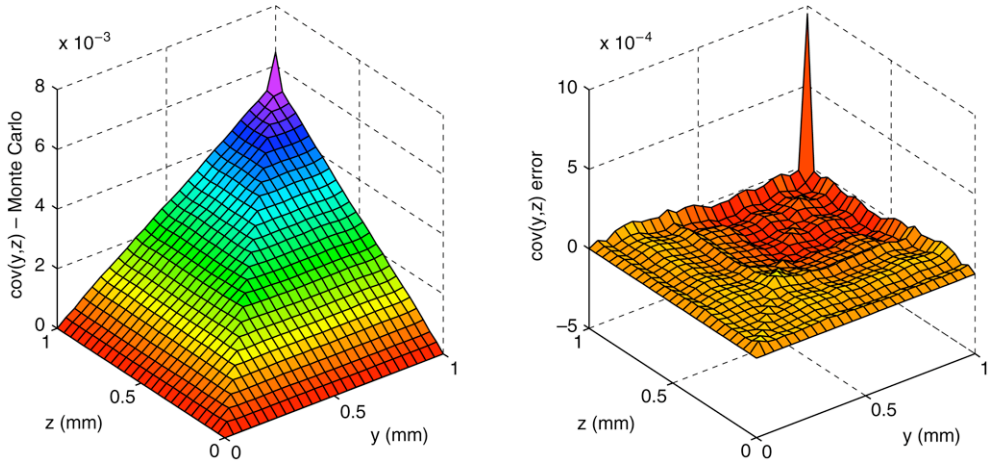

Fig. 10. Crack process covariance function: (a) covariance function of 5000 Monte Carlo simulations with $w = 0.5$ and $\lambda = 1000$, and (b) the error between the estimated covariance function and the approximate analytic covariance function in which positive values indicate that the MC result is larger than the analytic result.

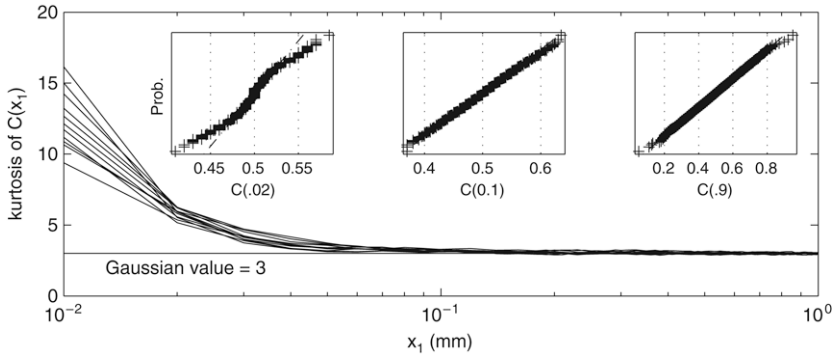

Fig. 11. Kurtosis of crack path process for $\lambda = 1000$ and $w = [0, 0.1, \ldots, 1]$ showing convergence to the Gaussian value of 3.0. Subframes show Gaussian probability plots for $C(x_1)$ with $w = 1$ at various positions, $x_1 = [0.02, 0.1, 0.9]$. The probability plots show that at $x_1 = 0.02$ the marginal distribution is far from Gaussian, but by $x_1 = 0.1$ the Gaussian distribution provides a high quality fit to the data.

occurs rapidly for the crack process. The main frame shows the kurtosis of $C(x_1)$ against position for $w = 0, 0.1, \ldots, 1.0$ and $\lambda = 1000$. Each curve is estimated from 5000 Monte Carlo simulations. The subframes show normal probability plots of the crack path process, again based on 5000 Monte Carlo simulations, for $w = 1$ at $x_1 = [0.02, 0.1, 0.9]$. By approximately $x_1 = 0.1$, the kurtosis and probability plots show excellent agreement with the Gaussian distribution. For $\lambda = 1000$, this corresponds to approximately 3 grain diameters.

4.4. Inhomogeneous polycrystals

The preceding results are for polycrystals in which $\lambda(\mathbf{x}) = \lambda$ is a constant, but it is well known that real materials exhibit spatially varying average grain sizes corresponding to spatially varying grain intensity $\lambda(\mathbf{x})$. Recall from the previous section the introduction of the normalized quantities $\tilde{x}_1(x_1) = \int_0^{x_1} \sqrt{\lambda} du$ and $\dot{s}^2 = \dot{\sigma}^2\sqrt{\lambda}$. These normalizations can be extended to the case where the intensity is a function of x_1 by

$$\tilde{x}_1 = \int_0^{x_1} \sqrt{\lambda(u)} du \text{ and}$$

$$\dot{s}^2(w) = \dot{\sigma}^2(w, x_1)\sqrt{\lambda(x_1)} \tag{13}$$

the second of which leads to a way to describe the variance growth of a crack process in an inhomogeneous polycrystal, which is now nonlinear. This description is

$$\sigma^2(w, x_1) = \int_0^{x_1} \frac{\dot{s}^2(w)}{\sqrt{\lambda(u)}} du \tag{14}$$

where $\dot{s}^2(w)$ can be found from Eq. (7) or Fig. 6.

To demonstrate the applicability of these expressions to inhomogeneous polycrystals, consider the following example. Let $\lambda(x_1) = 5000/(1+(2-x_1)^3)^2$ which produces polycrystals in which the average grain size decreases with x_1. That is, large grains are found near $x_1 = 0$ and small grains are found near $x_1 = 1$, similarly to the example of tessellation in Fig. 1(b). The average number of grains in such a polycrystal is 350. Assume also that $w = 0$ so that the maximum misorientation criterion is used to determine crack trajectories. From Eq. (7), $\dot{s}^2 = 0.5$ and Eq. (14) gives

$$\sigma^2(0, x_1) = \int_0^{x_1} \frac{1 + (2-u)^3}{10000} du = \frac{-36x_1 + 24x_1^2 - 8x_1^3 + x_1^4}{400\sqrt{2}}. \tag{15}$$

The variance of the crack process as estimated from 5000 Monte Carlo samples is shown in Fig. 12(b) along with the analytic solution for the crack process variance. The agreement is extremely good and indicates that the normalization scheme, as extended to inhomogeneous polycrystals, is correct. In the sample crack trajectories of Fig. 12(a), the decreasing grain size is observed in the shorter increments of crack advance as x_1 approaches 1. For the sake of brevity, a full investigation of the statistics of crack paths in inhomogeneous polycrystals is omitted from this paper, but the demonstrated correctness of Eq. (15) indicates that the statistics observed for cracks in homogeneous polycrystals should remain the same, excepting normalization by the instantaneous value of $\lambda(x_1)$. One extension to this study that is deferred at this time is the investigation of crack behavior in polycrystals in which the grain intensity depends on both x_1 and x_2.

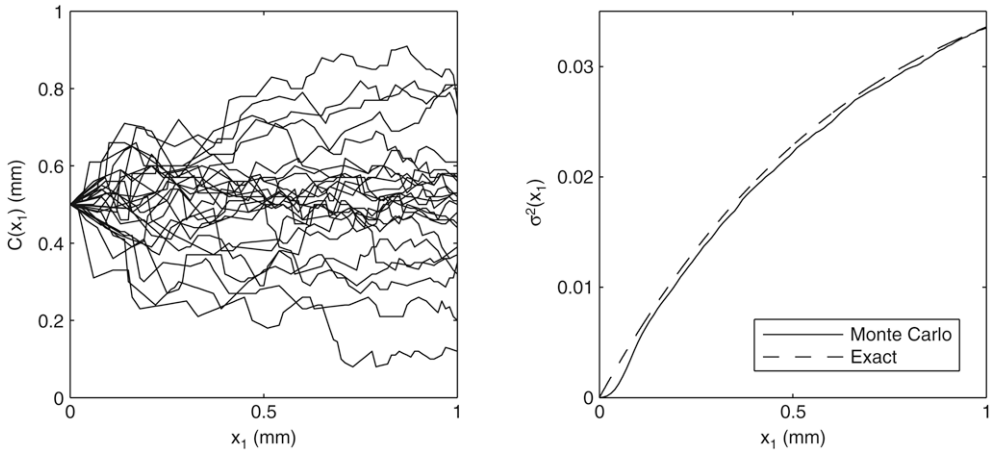

Fig. 12. Crack paths in inhomogeneous polycrystals: (a) crack trajectories and (b) variance growth of the crack process.

5. A model for intergranular cracks

The statistics presented in the previous section suggest a probabilistic model for intergranular cracks based on the incremental nature of the crack process. Let $C_i = C(X_{1,i}), i = 0, 1, \ldots$ be the position of the crack tip at locations $\{X_{1,i}\}$, such that $(C_i(X_{1,i}), X_{1,i})$ is the location of the ith vertex in the crack path process. The increments of the process are then given by

$$\begin{aligned} \Delta X_{1,i} &= X_{1,i} - X_{1,i-1} \\ \Delta X_{2,i} &= C_i - C_{i-1}, \quad i = 1, 2, \ldots \end{aligned} \tag{16}$$

which lead to

$$\begin{aligned} X_{1,i} &= x_{1,i-1} + \Delta X_{1,i} \quad \text{and} \\ C_i &= C_{i-1} + \Delta X_{2,i} \end{aligned} \tag{17}$$

as equations for the crack process.

To simulate the crack process, then, successive samples of the conditional random vector $[\Delta X_{1,i} \Delta X_{2,i}]^T | [\Delta X_{1,1} = \Delta x_{1,1}, \ldots, \Delta X_{1,i-1} = \Delta x_{1,i-1}; \Delta X_{2,1} = \Delta x_{2,1}, \ldots, \Delta X_{2,i-1} = \Delta x_{2,i-1}]$ are required. The difficulty posed by this expression is that the history vector grows with each successive step of crack advance. Fortunately, Monte Carlo results indicate that significant correlations do not extend past the previous increment, so that the actual task is merely to generate

$$[\Delta X_{1,i} \Delta X_{2,i}] | [\Delta X_{1,i-1} = \Delta x_{1,i-1} \Delta X_{2,i-1} = \Delta x_{2,i-1}] \tag{18}$$

which is easily accomplished using one of many methods for generating non-Gaussian random vectors (see, for example, [23–25]). To generate a statistically realistic intergranular crack, without generating a sample microstructure and without employing the propagation technique presented above, assuming $D = [0, a]^2$, specified w, specified grain intensity $\lambda(x_1)$, specified initiation site $C(0) = c_0$ and uniaxial macroscopic extension in the x_2 direction, the following steps can be followed:
Initialization phase:

(1) Find, from Eq. (7) or Fig. 6 the normalized rate of variance growth $\dot{s}^2$ for specified w,
(2) Find, from Figs. 8 and 9, the mean and variance of ΔX_1 and the correlation matrix of the random vector of Eq. (18),
(3) Generate a sample $\Delta x_{1,1}$ from the, approximately Weibull, random variable ΔX_1 with mean and variance taken from Fig. 8 and de-normalized by division by $\sqrt{\lambda(0)}$ and set $x_{1,1} = \Delta x_{1,1}$,
(4) Generate a sample $\Delta x_{2,1}$ from the two-sided exponential distribution with variance $\dot{s}^2(w)/\sqrt{\lambda(0)}\Delta x_{1,1}$ corresponding to $\nu = \sqrt{2/\dot{\sigma}^2 \Delta x_{1,1}}$ and which satisfies the cross correlation of $\Delta X_{2,1}$ with $\Delta X_{1,1}$, and set $c_1 = c_0 + \Delta x_{2,1}$.

Propagation, starting from $x_{1,1}$ and c_1, so that $i = 2, 3, \ldots$:

(5) Generate a sample $\Delta x_{1,i}$ from the, approximately Weibull, random variable ΔX_1 with mean and variance taken from Fig. 8 and de-normalized by division by $\sqrt{\lambda(x_{1,i-1})}$, and appropriate correlation with $\Delta x_{1,i-1}$ and $\Delta x_{2,i-1}$, and set $x_{1,i} = x_{1,i-1} + \Delta x_{1,i}$,
(6) Generate a sample $\Delta x_{2,i}$ from the two-sided exponential distribution with variance $\dot{s}^2(w)/\sqrt{\lambda(x_{1,i-1})}\Delta x_{1,1}$ corresponding to $\nu = \sqrt{2/\dot{\sigma}^2 \Delta x_{1,i}}$ and that satisfies the cross correlation of $\Delta X_{2,i}$ with $\Delta X_{1,i}$, $\Delta X_{1,i-1}$, and $\Delta X_{2,i-1}$, and set $c_i = c_{i-1} + \Delta x_{2,i}$,
(7) Repeat steps 5–6 until $x_i \geq a$.

To illustrate the effectiveness of this procedure, it is applied to the problem of generating synthetic crack trajectories for $D = [0, 1]^2$, $w = 0$, $\lambda = 1000$, $x_{1,0} = 0$, and $c_0 = 0.5$. Based on 5000 samples, Fig. 13 shows (a) example of synthetic crack trajectories that compare qualitatively well to those of Fig. 3(a), and (b) the variance of the synthetic crack process, that agrees well with the variance of the crack trajectories generated using the heuristic propagation criteria presented earlier.

This procedure generates synthetic crack trajectories that fully match the statistical properties of the Monte Carlo crack trajectories shown earlier. In some cases, it may be necessary only to know the location of the crack tip after a certain amount of overall crack advance rather than the full details of the crack tip history, namely the tortuous crack path. In such cases, subject to the same assumptions as above, a simple, but accurate model for the crack tip position is

$$\begin{aligned} c(x_1) &\sim N\left(c_0, \sigma^2\right) \\ \sigma^2(w, x_1) &= \int_0^{x_1} \frac{\dot{s}^2(w)}{\sqrt{\lambda(u)}} \mathrm{d}u, \end{aligned} \tag{19}$$

so that simulation of the crack tip position requires only generation of a Gaussian random variable, provided that the final crack position is more than several grain diameters from the initiation site.

6. Conclusion

Treating intergranular cracking as a random process, the numerical experiment of Monte Carlo simulation is used to estimate the statistical properties of intergranular microcracks. Due to the large number of realizations needed to provide reliable estimates of crack process statistics, a simplified heuristic for intergranular crack propagation in two-dimensional polycrystals is used that incorporates the effects of stress on grain boundary

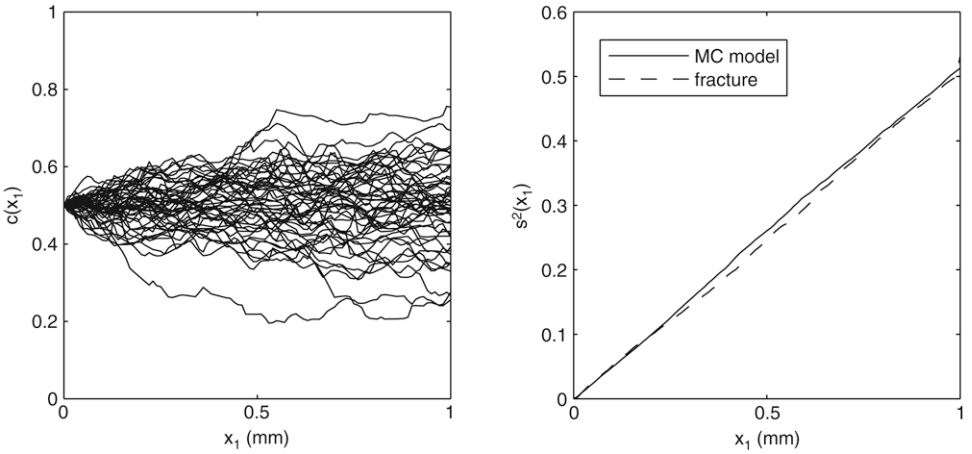

Fig. 13. Results of probabilistic crack mode for $D = [0, 1]^2$, $w = 0$, $\lambda = 1000$, $x_{1,0} = 0$, and $c_0 = 0.5$ showing, (a) sample crack trajectories, and (b) crack process variance compared against that for crack trajectories generated using heuristic propagation criteria.

faces and the fracture toughness of grain boundaries through the crystallographic orientation. In performing the Monte Carlo simulations, it is assumed that the cracks propagate through a polycrystal occupying the unit square $[0, 1]^2$ mm subject to uniaxial extension, and that the cracks do not branch and do not arrest. The polycrystals are modeled as Poisson–Voronoi tessellations in which the grains have orientation drawn from a uniform orientation distribution function.

The crack process exhibits linear variance growth, which is a property of random processes which are the sum of identically distributed random increments. The rate of variance growth depends on a parameter in the propagation heuristic that controls the relative importance of the stress acting on a grain boundary and the misorientation at the grain boundary in determining the direction of crack propagation. The rate of variance growth also depends on the grain size in the polycrystal such that the crack tip position is less uncertain in polycrystals with small grain sizes. This is believed to be a finding previously unreported, and adds to the well-known property of increased strength for small-grained polycrystals.

If the crack path is treated as an incremental process, the increments are found to be approximately Weibull and exponential for the crack tip advance increment and the crack tip diffusion increment respectively. The increments are found to be cross correlated, and also exhibit correlation between sequential increments, indicating that the crack path process cannot be modeled as one with independent increments. Despite this correlation of the crack process increments, the process is found to have Gaussian marginal distribution after the first few increments of crack advance and to have a scaled covariance function that closely resembles that of the Brownian motion process.

While the majority of results presented in this paper are for polycrystals that have spatially homogeneous average grain size, it is shown that a simple extension to the normalization of the crack statistics allows the same characterizations to be applied to polycrystals with spatially varying average grain sizes. Finally, a simple probabilistic model is presented that replicates the statistics of intergranular crack trajectories, and gives the ability to rapidly generate large numbers of synthetic cracks. Such a model should prove useful in investigations of the sensitivity of macrocracking problems to initial microcrack conditions, as well as providing statistically realistic microcracks with which to seed multi-scale fracture analyses.

The key issue left unresolved by this study is the relationship of the crack propagation parameter w to the actual mechanics of fracture, namely stress field heterogeneity and grain boundary fracture toughness. Also, a link between the crack path tortuosity and the energy required for fracture could provide insight into the fracture toughness of materials with variable grain size and differing distributions of grain boundary misorientation. Furthermore, a more realistic description of fracture in polycrystals should allow for crack branching and arrest, both of which must be heavily influential on the overall macroscopic fracture response of materials. Finally, it is not clear whether such an approach would be applicable to more realistic three-dimensional crack processes due to the increased geometrical complexity.

Acknowledgements

The authors acknowledge financial support for this work from the US National Science Foundation through grant #DMI-0423582. The comments of two anonymous reviewers were also valuable in improving the paper.

References

[1] Issa MA, Hammad AM, Chudnovsky A. Correlation between crack tortuosity and fracture toughness in cementitious material. International Journal of Fracture 1993;60:97–105.
[2] Anderson PM, Rice JR. Constrained creep cavitation of grain boundary facets. Acta Metallurgica 1985;33:409–22.
[3] Rice JR. Constraints on the diffusive cavitation of isolated grain boundary facets in creeping polycrystals. Acta Metallurgica 1981;29:675–81.
[4] van der Giessen E, Tvergaard V. Effect of random variations in microstructure on the development of final creep failure in polycrystalline aggregates. Modelling and Simulation in Materials Science and Engineering 1994;2:721–38.
[5] Xu XP, Needleman A. Numerical simulations of fast crack growth in brittle solids. Journal of the Mechanics and Physics of Solids 1994;42:1397.
[6] Zhou FH, Molinari JF, Shioya T. A rate dependent cohesive model for simulating dynamic crack propagation in brittle materials. Engineering Fracture Mechanics 2005;72:1383–410.
[7] Iesulauro E, Heber G, Wawrzynek P, Ingraffea AR. Modeling of 3d metallic polycrystals and simulation of crack initiation. In: International conference on computational engineering and sciences, 2002.
[8] Liu H, Arwade SR, Igusa T. Random composites classification and damage estimation using Bayesian classifiers. ASCE Journal of Engineering Mechanics 2007;133:129–40.
[9] Tan L, Arwade S. Response classification of simple polycrystalline microstructures. Computer Methods in Applied Mechanics and Engineering 2008;197:1397–409.
[10] Rao BN, Rahman S. Stochastic meshless analysis of elastic plastic cracked structures. Computational Mechanics 2003;32:199–213.
[11] Rao BN, Rahman S. Mesh-free analysis of cracks in isotropic functionally graded materials. Engineering Fracture Mechanics 2003;70:1–27.
[12] Zhang ZYJ, Paulino GH. Cohesive zone modeling of dynamic failure in homogeneous and functionally graded materials. International Journal of Plasticity 2005;21:1195–254.
[13] Brandinelli L, Ballarini R. Stress intensity factor approximations for two dimensional curvilinear cracks. Composite Science and Technology 2000;82:274–80.

[14] Ballarini R, Grigoriu M. Crack propagation in a material with random toughness. International Journal of Fracture 2004;125:353–69.
[15] Stoyan D, Kendall WS, Mecke J. Stochastic geometry and its applications. Chichester (England): Wiley; 1995.
[16] Randle V. The measurement of grain boundary geometry. Bristol (UK): Institute of Physics; 1993.
[17] Bunge H-J. Texture analysis in materials science. London: Butterworths; 1982.
[18] Anderson TL. Fracture mechanics: Fundamentals and applications. 2nd ed. Boca Raton (FL): CRC Press; 1995.
[19] Arwade SR. Stochastic characterization and simulation of material microstructures with application to aluminum. Ph.D. thesis, Ithaca (NY): Cornell University; January 2002.
[20] Arwade SR, Grigoriu M. A probabilistic model for polycrystalline microstructures with application to intergranular fracture. ASCE Journal of Engineering Mechanics 2004;130:997–1005.
[21] Kurishita H, Kuba S, Kubo H, Yoshinga H. Misorientation dependance of grain boundary fracture in molybdenum bicrystals with various ⟨110⟩ twist boundaries. Transactions of the Japan Institute of Metals 1985;26: 332–240.
[22] Li GH, Zhang LD. Relationship between misorientation and bismuth induced embrittlement of [001] tilt boundary in copper bicrystal. Scripta Metallurgica et Materialia 1995;32:1335–40.
[23] Arwade S. Translation vectors with non-identically distributed components. Probabilistic Engineering Mechanics 2005;20:158–67.
[24] Ferrante FJ, Arwade S, Graham-Brady LL. A translation model for non-stationary, non-Gaussian random processes. Probabilistic Engineering Mechanics 2005;20:215–28.
[25] Grigoriu M. Applied non-Gaussian Processes: Examples, theory, simulation, linear random vibration and MATLAB solutions. Englewood Cliffs (NJ): Prentice–Hall; 1995.